Non-aqueous bonding of leuprorelin to Ochratoxin A for solid-phase extraction

Naoki Yamato,[b] Noriaki Kumagai,[b] Momoha Okahira,[b] Satoru Kosaka,[b] Shuji Kodama,[d] Ryohei Yamamoto,[b] Atsushi Yamamoto,[b] Koichiro Takao[c] and Masanori Yamamoto[abc]*

Submitted 8th August 2022,

The anticancer leuprorelin was found to have excellent affinity to ochratoxin A (OTA), with an equilibrium constant of 2.2 × 10^8 M^{-1} at 273 K (dissociation constant K_d = 4.5 nM) when functionalized into a mesoporous polymer for binding to OTA. Binding between the surface-bound leuprorelin and mycotoxin was corroborated using DFT-based analysis, and it was extended to extraction of OTA from heavily fatty matrices of coffee, achieving 95% recovery with improved cyclability as compared with immunoaffinity.

Mycotoxins are natural toxins produced by fungi, and are adventitiously introduced into poultry and food-supply chains to threaten human health.[1-3] In particular, worldwide contamination of agricultural products by ochratoxin A (OTA, Fig. 1), which is a potent carcinogen with nephrotoxicity and heptatotoxicity,[2] is a serious concern in grains, beans (including coffee), and wine.[4-7] Inhibition of mycotoxin synthesis[8] has been studied to solve these issues, but the more practical method is to efficiently detect the chemicals at the boundaries of the food supply. However, foods contain various chemical compounds that hinder their detection using conventional techniques, including spectroscopy or mass spectrometry:[7,10] The detection of OTA requires sample clean-up prior to analysis. For example, coffee beans contain a large number of fatty ingredients that take in various phytochemicals such as 5~10wt% of chlorogenic acids,[11] 1~2wt% of caffeine,[12,13] lignans,[13] alkaloid trigonelline,[13] vitamin B_3 (niacin),[13] and other quinic acids.[14] As such, the facile and efficient separation of OTA from highly contaminated food matrices will be of great importance in analytical chemistry benefiting human health. The use of immunoaffinity,[15] aptamers,[16-28] metal–organic frameworks,[29] microporous MgO,[6] mesoporous silica,[30] graphene oxides,[31] nanocarbon materials,[32] DNA,[33] and other polymer nanoparticles[34] has been studied extensively to achieve high affinity toward OTA. However, the non-specific adsorption[16] can be significant in aqueous solutions as in the case of bovine serum albumin (BSA),[35] which could hinder the efficient separation of OTA from heavily contaminated food matrices. Thus, the development of non-aqueous molecular interactions with OTA is desired for efficient and facile separation.

In nature, human serum albumin (HSA)[36-39] has been reported to have a binding pocket for capturing OTA.[38,39] It is composed of basic residues, including tryptophan (Trp) and arginine (Arg), and hydrophobic residues such as valine (Val). Since the first reported solid-state peptide synthesis,[42] extensive research has greatly expanded the peptide library.[40,41] An appropriate synthetic peptide with the aforementioned residues would enable efficient capture of OTA even in non-aqueous solutions without the effect of denaturation-induced deactivation. Among the peptides available with Trp, Arg, and Val, we selected leuprorelin[43] (**1**, Fig. 1), a peptide comprising nine residues, as the binding model for efficient capture of OTA. **1** has a tyrosine (Tyr) unit, which is promising for anchoring the peptide to a porous resin through a covalently linked ether bridge formed by the S_N2 reaction of phenolic hydroxyl groups.[44]

To understand the molecular association in a homogeneous system, we first carried out spectroscopic analyses of an OTA solution in the presence of **1** at various concentrations. As shown in Fig. 2a, the pristine OTA solution in acetonitrile showed emission in the visible with a maximum at 451nm (purple line), while the addition of **1** shifted the peak maxima to 465 nm (red line) with two "isosbestic" points at 399 and 431 nm. The presence of isosbestic points suggests a possible equilibrium between free OTA and the OTA/**1** complex without any other species involved in the equilibrium. It is noteworthy that spectroscopic changes occurred even at low concentrations (25 nM for OTA and 0.1–1.6 μM for **1**). The enhanced emission is due to the structural change of OTA and/or the change in the dielectric constant of the surrounding environment from polar acetonitrile to the less polar peptide scaffold, which increases the transition probability in the radiative decay of a singlet excited state[45] upon association with **1**. This also supports the strong interaction and complexation of the OTA/**1** pair. The Hill plot[46] of the obtained spectroscopic results predicted 1:1 complexation (Fig. 2b) with a slope of ca. 1 and a correlation coefficient (R^2) of 0.986, while the Benesi–Hildebrand plot[47] based on Eq. 1

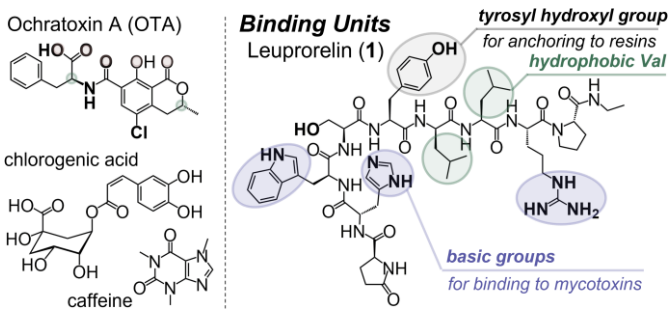

Fig. 1 Molecular structures of target substrates and leuprorelin (1) for the selected binding unit.

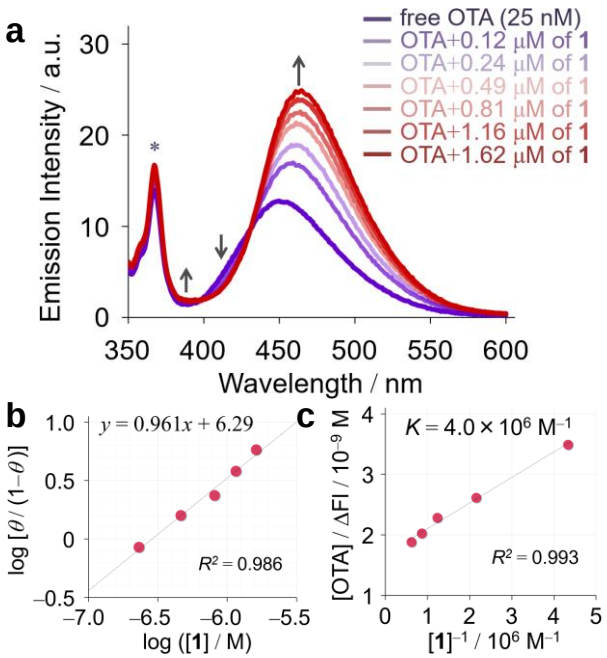

Fig. 2 (a) Steady-state emission spectra of the mycotoxin in wet acetonitrile in the presence of various concentrations of leuprorelin (1) at 297 K. The excitation wavelength was 330 nm. Raman scattering of the solvent is labeled with an asterisk. The spectral changes were sensitive to experimental conditions, and details are described in the ESI. (b) The Hill plot and (c) the Benesi–Hildebrand plot for OTA+1 derived from Figure 2a.

$$\frac{[\mathrm{OTA}]}{\Delta \mathrm{FL}} = \frac{1}{K[\mathbf{1}]} \bullet \frac{1}{c_{eq} - c_0} + \frac{1}{c_{eq} - c_0} \qquad (1)$$

gave an equilibrium constant of 4.0×10^6 M^{-1} at 297 K (Fig. 2c). In Eq. 1, [OTA] is the initial concentration of OTA, ΔFL is the difference in the emission intensity of OTA at a specified wavelength upon the addition of **1**, K is the binding constant in M^{-1}, [**1**] is the concentration of added **1**, and $(c_{eq} - c_0)^{-1}$ is a constant (for a detailed derivation of the Hill equation and Benesi–Hildebrand equation, see ESI†).

The binding constant of 10^6 M^{-1} is almost the same order as those of albumin[48] and aptamers[24] in aqueous buffer. With this in mind, **1** was then functionalized into the surfaces of a mesoporous resin by an S_N2 reaction between the phenolic oxygen and resin-bound epoxides (Fig. 3a) using a procedure analogous to the previously reported method,[44] for solid-phase extraction with the resin-bound analogue: In the presence of **1** (1.2 mM) and excess triphenyl phosphine (PPh_3), the suspension of the base resin (EG40) in *N*,*N*-dimethylformamide (DMF) was stirred at 110 °C for 4 h under a steady flow of Ar in the dark. The end of the reaction was determined using HPLC analysis. The obtained resin was extensively washed with methanol and toluene using a Soxhlet extractor, and then dried to obtain *poly***1**. The obtained material was characterized by elemental analysis, titration of the functionalized amino acids (Table S1),[49,50] and the adsorption isotherms for the gas phase (Fig. S2 and Table S2) and liquid phases (Figs. 3b).

Elemental analysis of nitrogen for the prepared *poly***1** showed the introduction of 21 μmol g^{-1} of **1** into the resin architecture, and the successful linkage between **1** and EG40 *via* the phenoxy unit of the Tyr residue was confirmed by the absence of Tyr in the hydrolyzed solution (Table S1). The nitrogen adsorption isotherm at 77 K showed retention of mesoporosity in *poly***1** after functionalization (Fig. S2 and Table S2). The affinity of OTA as an adsorbent for *poly***1** was investigated by determining the adsorption isotherms in the liquid phase using acetonitrile as the initial solvent. The temperature of the solution severely affected the thermodynamic parameters; therefore, the temperature of the system was carefully controlled during the investigation. When *poly***1** was dispersed in an acetonitrile solution of OTA, the emission from OTA decreased to a level close to zero within 2 h (Fig. S3) following an intraparticle diffusion model (*vide infra*). Fig 3b shows a sharp slope at extremely low concentrations (< 5 nM) of OTA for the *poly***1**/OTA pair. In contrast, when a polymer without functionalization of **1** was used instead of *poly***1**, almost no change was observed in the emission spectra. This accounts for spontaneous complexation between *poly***1** and OTA at the interfaces being thermodynamically favorable. The adsorption isotherms of *poly***1** at 273 K showed bi-Langmuir behavior in acetonitrile (Figs. 3b and S4), and the analysis gave the association constants of 2.2×10^8 M^{-1} for the "stronger" mode (as K_1) and 32 M^{-1} for the "weaker" mode (as K_2) (Fig. 3b). The former value is one-order of magnitude larger than previously reported well-sophisticated systems using aptamer[24] with K of 1.6×10^7 M^{-1} and polyaniline Langmuir-Blodgett film[27] with K of 1.2×10^7 M^{-1}.

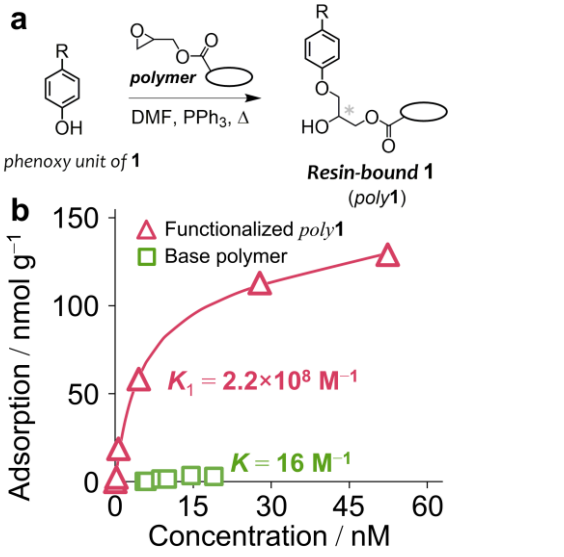

Fig. 3 (a) Schematic of the synthesis of *poly***1**. (b) Adsorption isotherms using OTA as an adsorbate in the presence of *poly***1** (triangle) or the corresponding unfunctionalized polymer (square) as the adsorbent at 273 K in acetonitrile. The vertical axis shows the amount of the adsorbed substrate per gram of a polymer, while the horizontal axis shows the equilibrium concentration of the substrate in the solution. *poly***1** gave a bi-Langmuir plot with K_1 = 2.2×10^8 M^{-1} and K_2 =32 M^{-1}. For more details, see Fig. S4 in the ESI†.

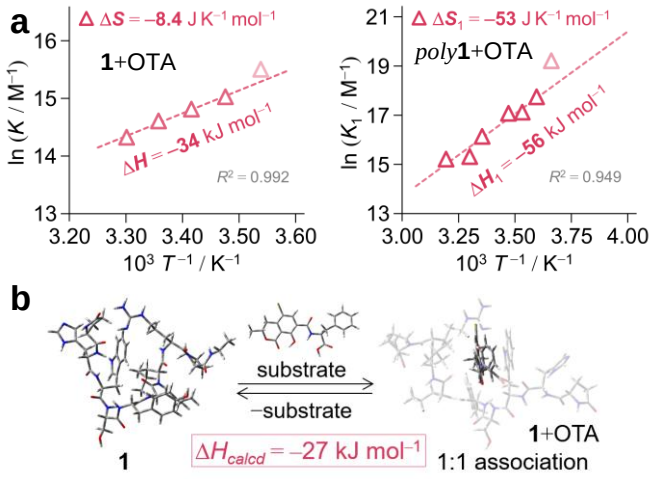

Fig. 4 (a) van't Hoff plot of ln *K* for homogeneous **1**+OTA pair (left) and heterogeneous pair with *poly***1** as a stationary phase and OTA as a substrate in acetonitrile (right). In both cases, the data set at 273 K largely deviated from the linear plot, and therefore, the analysis was conducted in temperatures higher than 278 K. The original data are shown in Figs. S1 and S4 of the ESI†. (b) Schematic shows the 1:1 association between **1** and OTA in acetonitrile computed by DFT method.

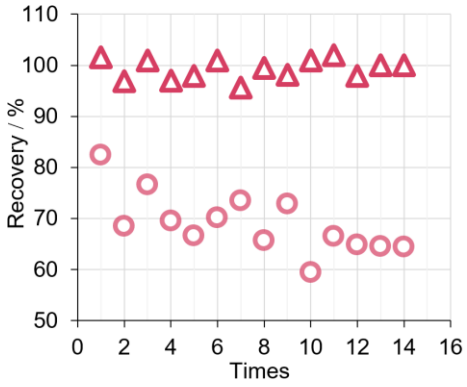

Fig. 5 Retention of OTA recovery using *poly***1** (triangle) and a commercially available immunoaffinity column (circle) with otherwise identical conditions.

Thus, functionalized **1** (*poly***1**) showed excellent binding to OTA in acetonitrile, but the details at the molecular level remain unclear. To further analyze the results, a van't Hoff plot[51] was obtained using the binding constants for the homogeneous and heterogeneous adsorbent/adsorbate pairs in a narrow range of temperatures (Figs. S1 and S4). Figs. 4ab shows the relationship between the logarithm of *K* and the reciprocal of temperature, which follows Eq. 2:

$$\ln K = -\Delta H/RT + \Delta S/R \qquad (2)$$

where ΔH is the enthalpy change of a reaction (herein the adsorption and desorption events, in J mol^{-1}), ΔS is the entropy change in J K^{-1} mol^{-1}, T is the temperature in K, and R is the gas constant (8.314 J K^{-1} mol^{-1}). The van't Hoff plot for the homogeneous pair gave ΔH of –34 kJ mol^{-1} and ΔS of –8.4 J K^{-1} mol^{-1} (Fig. 4a left). DFT calculation (Fig. 4b) corroborated the 1:1 binding of the homogeneous pair, as suggested by the Hill plot (Fig. 2b), with a computed ΔH_{calcd} value of –27 kJ mol^{-1}. On the contrary, the relationship for the heterogeneous "stronger" association showed a quasi-linear behavior with R^2 = 0.949 in a narrow temperature range, with ΔH_1 of –56 kJ mol^{-1} and ΔS_1 of –53 J K^{-1} mol^{-1}, respectively (Fig. 4a right). For the heterogeneous pair, the sparse surface functionalization of **1** (0.09 *per* square nanometer, Table S2) would support 1:1 binding even at the interfaces. As such, the larger heat of association at the interfaces (–56 kJ mol^{-1}) compared with that for the homogeneous pair (–34 kJ mol^{-1}) could be rationalized by the additional interactions with unobtrusive sites of the polymer units. In fact, the entropic contribution for the "stronger" binding (ΔS_1 = –53 J K^{-1} mol^{-1}) was highly negative toward the association compared to the corresponding homogeneous molecular system (ΔS = –8.4 J K^{-1} mol^{-1}), and this could be rationalized by the conformational changes upon association with OTA. That is, the approach of OTA may cause the induced fit of *poly***1**, and this requires an additional loss of conformational freedom within *poly***1**, leading to a decrease in ΔS_1. This interpretation supported the polymer-assisted association of OTA with *poly***1**.

When phosphate-buffered saline (PBS) was used instead of acetonitrile, the binding constant was substantially small (9.0 × 10^2 M^{-1}) for the *poly***1**/OTA pair at 273 K (Fig. S5). This sharp contrast (acetonitrile *versus* PBS) enabled selective capturing/release for efficient separation of OTA from food matrices with 95% of recovery (Fig. S6). In addition, iterative capture and release of OTA was achieved using *poly***1** with excellent durability (Fig. 5). This is in contrast to the use of a commercially available immunoaffinity column showing poor extraction of OTA from the corresponding coffee bean matrix (Fig. S6) and a gradual decrease in capturing/releasing efficiency (Fig. 5), validating the advantage of using peptides rather than proteins. Thus, the use of acetonitrile improved the solubility of organic molecules and thereby suppressed non-specific binding to unfunctionalized units of polymers, and this led to efficient and repeatable separation of OTA from food matrices.

Analysis of the solvent exchange kinetics of acetonitrile on the polymer followed the intraparticle diffusion (IPD) model,[52] and diffusion required longer times to achieve adsorption equilibrium (Figs. S7 and S8). In addition, the temperature dependence of the solvent exchange revealed that only a few percent of the pores were utilized for the liquid-phase events, even at 313 K (Table S3), compared to the total pore volume for micro- and mesopores determined by gas-phase adsorption isotherms using N_2 at 77 K. The limited diffusion restricts the maximum sites for

Table 1 Thermodynamic parameters for the association/dissociation equilibrium in acetonitrile and PBS (the equilibrium constant K in M^{-1}, the enthalpy change ΔH in kJ mol^{-1}, and the entropy change ΔS in J K^{-1} mol^{-1}) at 273 K unless otherwise noted.

set	in acetonitrile			in PBS
	K / M^{-1}	ΔH / kJ mol^{-1}	ΔS / J K^{-1} mol^{-1}	K / M^{-1}
1+OTA (283 K)	5.5 × 10^6	–34^a (–27)^b	–8.4^a	9.9 × 10^4
*poly***1**+OTA, K_1	2.2 × 10^8	–56^a	–53^a	9.0 × 10^2

^{a} These values were derived from the van't Hoff plot between 283 and 313 K as shown in Fig. 4a; ^{b} the value in parenthesis was calculated by computational chemistry using DFT method with PCM(acetonitrile) for implicit solvation.

adsorption (θ_{sat} ~ 100 nmol g^{-1} for the strong binding sites as shown in Fig. 3). Nevertheless, this study successfully demonstrated the binding between peptide **1** and OTA, even at the interfaces after its functionalization to porous materials, and this enabled us to quantify OTA extracted from coffee beans. The use of other porous materials, including porous graphene materials,[53] with improved porosity in the liquid phase and smaller secondary particle sizes will enhance OTA separation efficiency in the future.

In conclusion, we found efficient non-aqueous interactions between the anticancer therapeutic leuprorelin (**1**) and ochratoxin A (OTA). The homogeneous interaction between **1** and OTA shows a binding constant of 10^6 M^{-1} in acetonitrile, while the fixation of **1** onto the surfaces of a mesoporous polymer resulted in stronger binding sites to OTA with a binding constant of 10^8 M^{-1} at 273 K. Thermodynamic analysis and DFT calculations revealed that 1:1 binding occurred between **1** and the mycotoxin even at the functionalized polymer interface, and this could facilitate the efficient extraction of OTA from food matrices, including fatty mixtures extracted from coffee beans, with improved reusability.

This work was supported by Grant-in-Aids (18K05526). Computational chemistry was investigated at the Research Center for Computational Science, Institute for Molecular Science, Okazaki, Japan (Project: 21-IMS-C263).

Author Affiliation

[a] *Institute of Multidisciplinary Research for Advanced Materials Tohoku University, 2-1-1 Katahira, Aoba, Sendai 980–8577, Japan*
E-mail: yamamoto@mol-chem.com
[b] *College of Bioscience and Biotechnology, Chubu University Matsumoto 1200, Kasugai, Aichi 487–8501, Japan*
[c] *Laboratory for Zero-Carbon Energy, Institute of Innovative Research, Tokyo Institute of Technology, Ookayama 2-12-1, Meguro, Tokyo, 152–8550, Japan*
[d] *School of Science, Tokai University*
4-1-1 Kitakaname, Hiratsuka, Kanagawa 259-1292, Japan

Conflicts of interest

There are no conflicts to declare.

Notes and references

1. F. J. Hoerr, *Mycotoxicoses* in *Diseases of Poultry*, *14th Edition*, John Wiley & Sons, Inc., 2020, Chapter 31, 1330-1348.
2. M. S. Samuel, K. Jeyaram, S. Datta, N. Chandrasekar, R. Balaji and E. Selvarajan, *J. Agric. Food. Chem.*, 2021, **69**, 13974-13989.
3. J. L. Richard, *Int. J. Food Microbiol.*, 2007, **119**, 3-10.
4. S. D. Stoev, *Toxicon*, 2021, **190**, 41-49.
5. H. Yan, L. Zhang, Z. Ye, A. Wu, D. Yu, Y. Wu and Y. Zhou, *J. Agric. Food. Chem.*, 2021, **69**, 12021-12029.
6. M.-N. Nan, Y. Bi, Y. Qiang, H.-L. Xue, L. Yang, L.-D. Feng, L.-M. Pu, H.-T. Long and D. Prusky, *Food Chem.*, 2022, **371**, 131157.
7. R. Yamamoto, M. Sawada, N. Yamato, A. Yamamoto and S. Kodama, *Sep. Sci. Plus*, 2018, **1**, 196-201.
8. T. Furukawa, H. Katayama, A. Oikawa, L. Negishi, T. Ichikawa, M. Suzuki, K. Murase, S. Takayama and S. Sakuda, *Cell Chem. Biol.*, 2020, **27**, 1396-1409.e1310.
9. L. S. Ettre, *LC GC North America*, 2001, **19**, 506-512.
10. N. Pallarés, H. Berrada, G. Font and E. Ferrer, *J. Food Sci. Technol.*, 2021, DOI: 10.1007/s13197-021-05306-y.
11. R. Lang, S. Klade, A. Beusch, A. Dunkel and T. Hofmann, *J. Agric. Food. Chem.*, 2015, **63**, 10492-10499.
12. G. P. Fox, A. Wu, L. Yiran and L. Force, *J. Agric. Food. Chem.*, 2013, **61**, 10772-10778.
13. R. M. van Dam, F. B. Hu and W. C. Willett, *N. Engl. J. Med.*, 2020, **383**, 369-378.
14. K. Tanaka, S. Nishizono, S. Tamaru, M. Kondo, H. Shimoda, J. Tanaka and T. Okada, *Food Sci. Technol. Res.*, 2009, **15**, 147-152.
15. S. Höfs, D. Hülagü, F. Bennet, P. Carl, S. Flemig, T. Schmid, J. A. Schenk, V.-D. Hodoroaba and R. J. Schneider, *ChemElectroChem*, 2021, **8**, 2597-2606.
16. J. A. Cruz-Aguado and G. Penner, *J. Agric. Food. Chem.*, 2008, **56**, 10456-10461.
17. Y. Li, R. Su, H. Li, J. Guo, N. Hildebrandt and C. Sun, *Anal. Chem.*, 2022, **94**, 193–224.
18. H. Yu, O. Alkhamis, J. Canoura, Y. Liu and Y. Xiao, *Angew. Chem. Int. Ed.*, 2021, **60**, 16800-16823.
19. O. Alkhamis, J. Canoura, K. V. Bukhryakov, A. Tarifa, A. P. DeCaprio and Y. Xiao, *Angew. Chem. Int. Ed.*, 2022, **61**, e202112305.
20. J. Canoura, H. Yu, O. Alkhamis, D. Roncancio, R. Farhana and Y. Xiao, *J. Am. Chem. Soc.*, 2021, **143**, 805-816.
21. B. Billet, B. Chovelon, E. Fiore, F. Oukacine, M.-A. Petrillo, P. Faure, C. Ravelet and E. Peyrin, *Angew. Chem. Int. Ed.*, 2021, **60**, 12346-12350.
22. D. E. Armstrong-Price, P. S. Deore and R. A. Manderville, *J. Agric. Food. Chem.*, 2020, **68**, 2249-2255.
23. Y. Li, N. Zhang, H. Wang and Q. Zhao, *J. Agric. Food. Chem.*, 2020, **68**, 4277-4283.
24. A. V. Samokhvalov, I. V. Safenkova, S. A. Eremin, A. V. Zherdev and B. B. Dzantiev, *Anal. Chem.*, 2018, **90**, 9189-9198.
25. P. S. Deore, M. D. Gray, A. J. Chung and R. A. Manderville, *J. Am. Chem. Soc.*, 2019, **141**, 14288-14297.
26. L. Li, S. Xu, H. Yan, X. Li, H. S. Yazd, X. Li, T. Huang, C. Cui, J. Jiang and W. Tan, *Angew. Chem. Int. Ed.*, 2021, **60**, 2221-2231.
27. N. Prabhakar, Z. Matharu and B. D. Malhotra, *Biosens. Bioelectron.*, 2011, **26**, 4006-4011.
28. S. Zhang, Y. Luan, M. Xiong, J. Zhang, R. Lake and Y. Lu, *ACS Appl. Mater. Interfaces*, 2021, **13**, 9472-9481.
29. S. Hu, W. Ouyang, L. Guo, Z. Lin, X. Jiang, B. Qiu and G. Chen, *Biosens. Bioelectron.*, 2017, **92**, 718-723.
30. C. Hofmann, A. Duerkop and A. J. Baeumner, *Angew. Chem. Int. Ed.*, 2019, **58**, 12840-12860.
31. Z. Bytesnikova, V. Adam and L. Richtera, *Food Control*, 2021, **121**, 107611.
32. P. K. Gupta, D. Chauhan, Z. H. Khan and P. R. Solanki, *ACS Appl. Nano Mater.*, 2020, **3**, 2506-2516.
33. W. Białobrzeska, M. J. Głowacki, M. Janik, M. Ficek, K. Pyrchla, M. Sawczak, R. Bogdanowicz, N. Malinowska, S. Żołędowska and D. Nidzworski, *J. Mol. Liq.*, 2021, **342**, 117338.
34. D. López-Puertollano, T. Cowen, Á. García-Cruz, E. Piletska, A. Abad-Somovilla, A. Abad-Fuentes and S. Piletsky, *ChemNanoMat*, 2019, **5**, 651-657.
35. K. Hirota, S. Hashida, E. Ishikawa and M. Totani, *Ann. Clin. Biochem.*, 1998, **35**, 649-655.
36. S. Curry, H. Mandelkow, P. Brick and N. Franks, *Nat. Struct. Biol.*, 1998, **5**, 827-835.
37. J. Ghuman, P. A. Zunszain, I. Petitpas, A. A. Bhattacharya, M. Otagiri and S. Curry, *J. Mol. Biol.*, 2005, **353**, 38-52.
38. Y. V. Il'ichev, J. L. Perry and J. D. Simon, *J. Phys. Chem. B*, 2002, **106**, 452-459.
39. J. L. Perry, M. R. Goldsmith, M. A. Peterson, D. N. Beratan, G. Wozniak, F. Rüker and J. D. Simon, *J. Phys. Chem. B*, 2004, **108**, 16960-16964.
40. E. Lenci and A. Trabocchi, *Chem. Soc. Rev.*, 2020, **49**, 3262-3277.
41. F. Sheehan, D. Sementa, A. Jain, M. Kumar, M. Tayarani-Najjaran, D. Kroiss and R. V. Ulijn, *Chem. Rev.*, 2021, **121**, 13869-13914.
42. R. B. Merrifield, *J. Am. Chem. Soc.*, 1963, **85**, 2149-2154.
43. M. Katsuno, H. Adachi, M. Doyu, M. Minamiyama, C. Sang, Y. Kobayashi, A. Inukai and G. Sobue, *Nat. Med.*, 2003, **9**, 768-773.
44. M. Yamamoto, M. Obara, K. Ochi, A. Yamamoto, K. Takenaka, T. Tanaka and K. Sato, *ChemPlusChem*, 2018, **83**, 820-824.
45. V. R. N. J. Turro and J. C. Scaiano, in *Principles of Molecular Photochemistry*, Univ Science Books, Sausalito, California, 2008, Chapter 4.
46. K. M. Kadish, P. Chen, Y. Y. Enakieva, S. E. Nefedov, Y. G. Gorbunova, A. Y. Tsivadze, A. Bessmertnykh-Lemeune, C. Stern and R. Guilard, *J. Electroanal. Chem.*, 2011, **656**, 61-71.
47. H. A. Benesi and J. H. Hildebrand, *Journal of the American Chemical Society*, 1949, **71**, 2703-2707.
48. Y. V. Il'ichev, J. L. Perry, F. Rüker, M. Dockal and J. D. Simon, *Chem. Biol. Interact.*, 2002, **141**, 275-293.
49. R. J. Simpson, M. R. Neuberger and T. Y. Liu, *J. Biol. Chem.*, 1976, **251**, 1936-1940.
50. Y. Ishida, T. Fujita and K. Asai, *J. Chromatogr. A*, 1981, **204**, 143-148.
51. J. D. Martell, P. J. Milner, R. L. Siegelman and J. R. Long, *Chem. Sci.*, 2020, **11**, 6457-6471.
52. F.-C. Wu, R.-L. Tseng and R.-S. Juang, *Chem. Eng. J.*, 2009, **153**, 1-8.
53. M. Yamamoto, Z. Qi, S. Goto, Y. Gu, T. Toriyama, T. Yamamoto, M. Tamura, K. Tomishige, A. Aziz, R. Crespo-Otero, D. D. Tommaso, T. Kyotani and K. Yamazaki, *Chem. Sci.*, 2022, **13**, 3140–3146.